AGU PUBLICATIONS

JGR

Journal of Geophysical Research: Solid Earth

RESEARCH ARTICLE
10.1002/2017JB013968

Key Points:
- CO_2 emissions from back-arc mud volcanoes are important sources within the geochemical carbon cycle and greenhouse gas budget
- The CO_2 flux of Bledug Kuwu back-arc mud volcano has been measured with a remote sensing spectrometer and compared with magmatic sources
- Potential sources for the CO_2 emitted from the mud volcano are considered

Supporting Information:
- Supporting Information S1
- Movie S1

Correspondence to:
M. Queißer,
manuel.queisser@manchester.ac.uk

Citation:
Queißer, M., M. R. Burton, F. Arzilli, A. Chiarugi, G. I. Marliyani, F. Anggara, and A. Harijoko (2017), CO_2 flux from Javanese mud volcanism, *J. Geophys. Res. Solid Earth*, *122*, 4191–4207, doi:10.1002/2017JB013968.

Received 10 JAN 2017
Accepted 7 MAY 2017
Accepted article online 9 MAY 2017
Published online 3 JUN 2017

CO_2 flux from Javanese mud volcanism

M. Queißer[1], M. R. Burton[1], F. Arzilli[1], A. Chiarugi[2], G. I. Marliyani[3], F. Anggara[3], and A. Harijoko[3]

[1]School of Earth and Environmental Sciences, University of Manchester, Manchester, UK, [2]Istituto Nazionale di Geofisica e Vulcanologia, Pisa, Italy, [3]Geological Engineering Department, Universitas Gadjah Mada, Yogyakarta, Indonesia

Abstract Studying the quantity and origin of CO_2 emitted by back-arc mud volcanoes is critical to correctly model fluid-dynamical, thermodynamical, and geochemical processes that drive their activity and to constrain their role in the global geochemical carbon cycle. We measured CO_2 fluxes of the Bledug Kuwu mud volcano on the Kendeng Fold and thrust belt in the back arc of Central Java, Indonesia, using scanning remote sensing absorption spectroscopy. The data show that the expelled gas is rich in CO_2 with a volume fraction of at least 16 vol %. A lower limit CO_2 flux of 1.4 kg s^{-1} (117 t d^{-1}) was determined, in line with the CO_2 flux from the Javanese mud volcano LUSI. Extrapolating these results to mud volcanism from the whole of Java suggests an order of magnitude total CO_2 flux of 3 kt d^{-1}, comparable with the expected back-arc efflux of magmatic CO_2. After discussing geochemical, geological, and geophysical evidence we conclude that the source of CO_2 observed at Bledug Kuwu is likely a mixture of thermogenic, biogenic, and magmatic CO_2, with faulting controlling potential pathways for magmatic fluids. This study further demonstrates the merit of man-portable active remote sensing instruments for probing natural gas releases, enabling bottom-up quantification of CO_2 fluxes.

Plain Language Summary Unlike volcanoes, mud volcanoes produce no lava but liquefied mud. However, similar to volcanoes, they emit various types of gases, including the greenhouse gas carbon dioxide (CO_2). To better understand mud volcanoes and their role in the global carbon cycle, a quantification of their CO_2 fluxes is critical. The island of Java (Indonesia) hosts many volcanoes and mud volcanoes with unknown CO_2 output. Given the particular geology of Java, mud volcanoes may be connected to volcanoes and CO_2 emitted by mud volcanoes may stem from the volcanic plumbing system. We measured CO_2 fluxes of the Bledug Kuwu mud volcano in Central Java, using a novel scanning remote sensing spectrometer, which enabled us to measure quickly and from a safe distance. Our findings show that the expelled gas is rich in CO_2 with a volume fraction of at least 16%. A lower limit CO_2 flux of 1.4 kg s^{-1} (117 t d^{-1}) was determined, in line with the CO_2 flux from the infamous Javanese mud volcano LUSI. After discussing geochemical, geological, and geophysical evidence we conclude that a fraction of the CO_2 observed at Bledug Kuwu may be sourced from volcanic magma.

1. Introduction

The concentration of CO_2 in the atmosphere is a result of anthropogenic and natural CO_2 sources and sinks. Natural sources include biogenic and geological processes such as metamorphic breakdown of carbonates and magmatic degassing. Our quantitative understanding of the global geochemical carbon cycle is underpinned by empirical observations of the fluxes of CO_2 produced by geological processes [*Le Cloarec and Marty*, 1993; *Burton et al.*, 2013; *Kelemen and Manning*, 2015]. Magmatic emissions from volcanic centers represent one of the key geological sources of CO_2 [*Olivier et al.*, 1996; *Gerlach et al.*, 2002; *Etiope et al.*, 2007, *Burton et al.*, 2013; *Lee et al.*, 2016].

Mud volcanism (MV) is produced by a combination of fault structures and sedimentary layers, often in back-arc areas, which produce CO_2 that is usually of a combined biogenic and geological origin. MV is the result of liquefied sediments and gases reaching the surface due to overpressure and buoyancy [*Milkov*, 2000; *Dimitrov*, 2002]. MV is a common feature in tectonically active regions with a predominantly compressive setting, such as in subduction zones. Thousands of mud volcanoes have been identified offshore [*Milkov*, 2000], and at least hundreds exist onshore [*Kopf*, 2002]. Their sheer number implies that subaerial MV may contribute significantly to the atmospheric CO_2 budget and hence the geochemical carbon cycle.

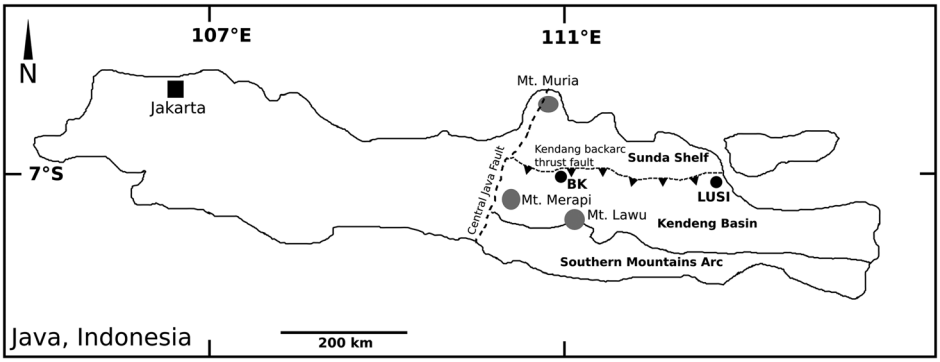

Figure 1. Map of Java, Indonesia, and the mud volcano Bledug Kuwu (abbreviated as BK). The geological features were compiled from *Smyth et al*. [2008] and *Setijadji* [2010].

Furthermore, owing to their common proximity to volcanic arcs, they may play a key role in the overall picture of back-arc CO_2 emissions associated with arc volcanism, together with fore-arc and arc volcano degassing [*Füri et al*., 2010, *Giammanco et al*., 2007; *Westbrook and Smith*, 1983]. Therefore, studying the role of volcanoes in the global carbon cycle should include investigating CO_2 emissions produced by MV. If CO_2 emitted by MV has a magmatic origin, the budget of mantle-derived CO_2 emitted by volcanism may have to be amended and models that describe carbon transfer from slab to mantle wedge and exosphere updated [*Kerrick and Connolly*, 2001; *Connolly*, 2005; *Gorman et al*., 2006; *Poli et al*., 2009].

The Indonesian archipelago located in the southern edge of Sundaland in Southeast Asia is extraordinarily rich for both arc volcanism and MV [*Barber et al*., 1986]. However, relatively limited CO_2 emission data are available. CO_2 emissions from these sources may contribute significantly to the country's total carbon emission, in addition to those of anthropogenic origin. Therefore, in addition to purely scientific goals, motivations to quantify natural CO_2 emission rates are hazard management and policy making regarding controls on Indonesian carbon emissions.

Measuring gas emission rates (mass fluxes) requires gas concentration profiles and the transport speed of the emitted gas. Owing to high background atmospheric concentrations, CO_2 concentration profiles are usually obtained from grids of in situ measurements [e.g., *Brantley and Koepenick*, 1995; *Shinohara*, 2005; *Hernández et al*., 2015]. These techniques are often time consuming and, especially at volcanic sites and mud volcanoes, bear a safety risk. Remote sensing techniques provide a safe distance and a spatially integrated measurement, yielding gas concentration profiles that can directly be used to compute gas fluxes. Remote sensing is an established technique to measure volcanic SO_2 fluxes [*Stoiber et al*., 1983; *Oppenheimer et al*., 1998; *Burton et al*., 2000; *Duffell et al*., 2001; *Galle et al*., 2003] and, along with in situ data of CO_2 concentration, is used in a routine fashion to indirectly retrieve volcanic CO_2 fluxes [*Gerlach et al*., 1998; *Burton et al*., 2013]. LIDAR technology has recently advanced sufficiently to allow direct remote sensing of volcanic CO_2 fluxes, independent of sunlight [*Aiuppa et al*., 2015; *Queißer et al*., 2016].

In this study CO_2 from the Bledug Kuwu mud volcano complex located in Central Java, Indonesia, was probed using a novel, portable CO_2 LIDAR. The large volume of mud extruded by this mud volcano limited access to the main vent area, making CO_2 flux determinations using in situ CO_2 measurement techniques challenging. This setting was therefore deemed ideal for a remote sensing instrument and, in particular, our recently developed CO_2 LIDAR system [*Queißer et al*., 2016], due to its flexibility, portability, and ease of use. The motivation for the campaign was twofold. First, the Bledug Kuwu MV complex underwent sampling of gas emission and composition [*Mazzini et al*., 2012], but CO_2 fluxes have yet not been measured and a connection to arc volcanism has yet not been discussed. Second, the measurement offered a possibility to deploy a man-portable active remote sensing instrument developed for volcanic CO_2 detection for the first time at a mud volcano.

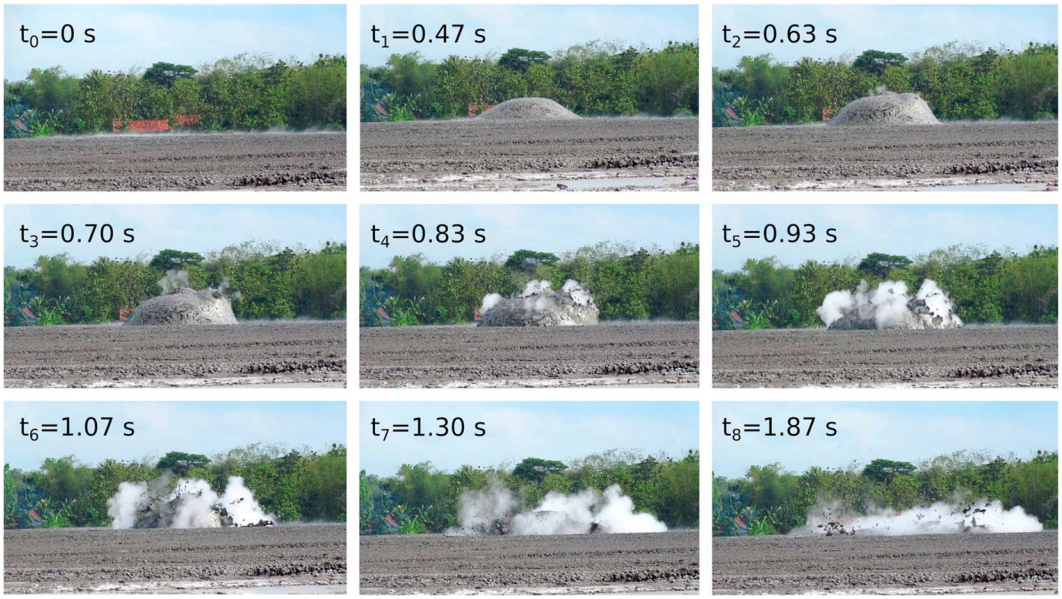

Figure 2. Snapshots of a bursting gas bubble of the main vent (vent II) at the Bledug Kuwu complex. The bursts had a duration of approximately ~2 s.

2. Geologic Setting of Bledug Kuwu

Bledug Kuwu is an active mud volcano located near the village of Kuwu in Central Java (Figure 1) in the back-arc region of the Java subduction system [*Whittaker et al*., 2007]. The subduction process and its associated arc volcanism shape the topography of Java [*Hall and Smyth*, 2008].

A lateral cross section of a subduction zone typically reveals a systematic series of components in the landward direction: accretionary prism, fore-arc basin, arc volcanism, and back-arc region. In Java the geometry of the back-arc regions varies but it generally forms an elongated E-W basin to the north of the volcanic arc. The basin is filled by rapid sedimentation of terrigenous material [*Smyth et al*., 2005]. Persistent compressive stresses deformed the sediments, developing an imbrication of fold and reverse faults observable today.

The topography of the back-arc region in the central and eastern part of Java is dominated by the prominent fold and thrust belt of Kendeng (Figure 1). Rapid sedimentation combined with the increasing stress from the subduction and vertical loading from the magmatic bodies creates favorable condition for the formation of MV [*Satyana and Asnidar*, 2008]. This is the area where Bledug Kuwu and other mud volcanoes are located, confined within a low relief zone. Within a radius of ~2 km around Bledug Kuwu are four other mud volcanoes: Cangkring Bleduk, Bleduk Banjarsari, Bleduk Crewek, and Medang Kamolan [*Istadi et al*., 2012]. The nearest active volcano is Mount Lawu, located about 60 km to the south of Bledug Kuwu as part of the volcanic arc (Figure 1).

The Bledug Kuwu mud volcano complex forms a low relief, nearly flat surface, about 700 m in diameter. The low relief of the crater and the dome indicates that the material is dominated by low viscosity sediments and that the fluidity of the material is maintained by the release of liquid and gasses [*Istadi et al*., 2012]. The active vent system consists of at least three eruption centers. Two main vents produce infrequent bursts of gas bubbles piercing the mud surface, forming semispherical shapes under the layer of mud, which then burst, splattering mud in all directions (Figure 2). Eruptions appear infrequent but occur at least twice a minute. The plume emitted at the main vents consists mainly of condensed water vapor that can be observed when the bubbles explode (Figure 2). The explosion is followed by a quasi-concentric movement of the plume front away from the center of the vent (Movie S1 in the supporting information) forming a ring pattern.

Seismic reflection profiles reveal that the disturbed zone associated with Bledug Kuwu is produced by the upper part of Kujung formation passing Wonocolo formation and breaking onto the surface [*Satyana and Asnidar*, 2008]. Analysis of microfossils contained within the solid material extruded by Bledug Kuwu indicates that the source of the mud is located in the lower part of late Miocene Wonocolo shales about 2 km deep

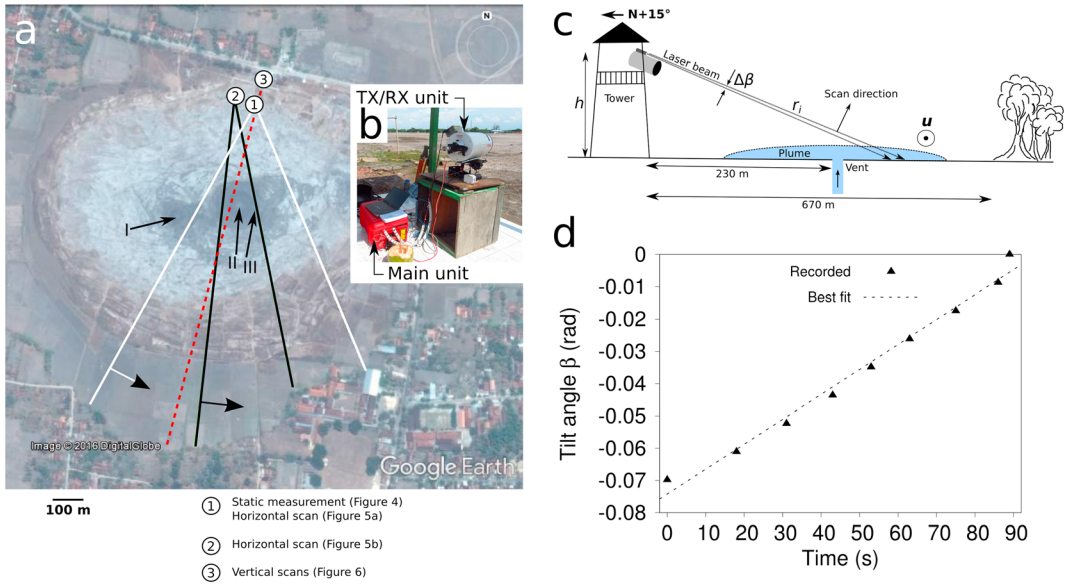

Figure 3. Overview of the measurement geometry at the Bledug Kuwu mud volcano complex and the CO_2 LIDAR used to remotely measure CO_2 column densities. (a) The three positions taken by the instrument for the different data. Lines indicate start and stop heading angles of the horizontal scans. Both horizontal scans were performed on 27 September 2016, while the vertical scans were carried out the 28 September 2016. The arrows perpendicular to the start angle lines indicate the anticlockwise scanning direction. Roman numbers and arrows point to the vents where emerging bubbles could be identified, with II being the main vent. The red dotted line depicts the plane for the vertical scans. (b) Photo of instrument while at position 1. (c) Scheme (not to scale) of the vertical scans depicting the instrument at position 3 (on the railing inside a tower), the main vent probed and the distribution of the gas plume, the plume transport speed (pointing perpendicular to the paper plane), and trees used as hard target, along with the ground. (d) Example of recorded tilt angles of TX/RX unit from a tilt meter and straight line fit.

[*Satyana and Asnidar*, 2008]. However, the seismic reflection data leave room for the possibility that the mud stems from early Miocene Tuban shales from 3 to 4 km depth.

3. Materials and Methods

3.1. The Measurement Instrument

The measurements at the Bledug Kuwu mud volcano field took place between the afternoon of the 27 September 2016 and morning of the 28 September 2016. The zone around the main vent of the mud field was probed using a purpose-built active laser remote sensing spectrometer, the CO_2 LIDAR [*Queißer et al.*, 2016]. It uses an ~ 1 W tunable near-infrared laser to illuminate a topographic feature behind the emitted gas and a receiver telescope to collect the backscattered radiation while the laser is tuned across a CO_2 absorption band at 1.57 μm. Figure 3a shows a map of Bledug Kuwu and the points where the instrument was located for the acquisitions. An earlier version of the CO_2 LIDAR has been described in detail in *Queißer et al.* [2016], but continuous development of the instrument means that the version used on Bledug Kuwu has some key differences. The remote sensing spectrometer consists of a main unit (Figure 3b) and the transmitter/receiver unit (TX/RX unit). The latter composes of the telescope, transmitter, and an integrating sphere for power reference measurement. A main difference to the previous instrument is that instead of interlacing two wavelengths on and off the CO_2 line, the CO_2 absorption line was sampled at 20 wavelengths by tuning the laser across the absorption line, such that the absorption maximum was located at the center of the wavelength sweep. A model absorption spectrum, the product of a background polynomial and the CO_2 transmittance curve, was fitted to the 20 measured transmittances resulting in a best estimate of the path-averaged CO_2 concentration. As shown by *Abshire et al.* [2010], this not only yielded additional information in terms of changes in baseline compared with the two-wavelength approach but also proved to be more robust to spectroscopic wavelength shifts and instrumental offsets due to wavelength dependencies (e.g., transmittance of instrument). In addition, for each retrieved value of CO_2 concentration an individual

spectrum and a meaningful estimate of the quality (confidence) of that value are provided through the model covariance matrix.

3.2. Measurement of CO_2 Column Densities

CO_2 column densities (in m^{-2}) were retrieved as

$$N^{\mathrm{col}} = \frac{\ln(\min(F))}{2\Delta\sigma}. \tag{1}$$

$\Delta\sigma$ is the molecular absorption cross sections of CO_2 associated with the wavelength corresponding to the absorption peak minus the absorption cross sections for the wavelength at minimum absorption (differential absorption cross section). F depicts the best fit transmittance, i.e., the fit of the transmittance values SR_j measured at given wavelengths λ_j (i.e., the spectrum). At a given wavelength, the spectrum was retrieved as

$$SR_j = \sum_{k=1}^{N_S} \frac{S_{jk}}{R_{jk}}, \tag{2}$$

where N_S is the number of spectra to stack (to increase the signal-to-noise ratio) and S and R represent the strength of the atmospheric return and the transmitted signal, respectively, measured at 20 discrete wavelengths $\lambda_j \in [1, 20]$. Although not used for the flux retrieval, for illustrative purposes, column-averaged path-averaged CO_2 mixing ratio (in ppm) were obtained from the column densities using

$$X_{CO_2} = \frac{N^{\mathrm{col}}}{rN_{\mathrm{air}}} 10^6, \tag{3}$$

where N_{air} (in m^{-3}) is the dry air number density computed with knowledge of specific humidity, air pressure, and temperature and r depicts the range to the hard target.

3.3. Retrieval of the CO_2 Flux

The CO_2 flux was computed as

$$\Phi_{CO_2} = u \frac{M_{CO_2}}{N_A} \Delta\beta \sum_{\mathrm{plume}} {N^{\mathrm{col}}}_{pl} r_i, \tag{4}$$

where u refers to the component of the plume transport speed perpendicular to the plane of the CO_2 concentration profile, i.e., the component perpendicular to the plane of the scan. M_{CO_2} is the molar mass of CO_2 (in kg mol^{-1}) and N_A is Avogadro's constant (in mol^{-1}). The constant scan angle increment $\Delta\beta$ was retrieved using the start and stop angles β_S and β_E of the scan as

$$\Delta\beta = \frac{\beta_E - \beta_S}{N_{\mathrm{Spec}}}, \tag{5}$$

where N_{Spec} depicts the total number of averaged spectra acquired during the scan. ${N^{\mathrm{col}}}_{\mathrm{pl}}$ is the background-corrected CO_2 column density (the plume column density) obtained as ${N^{\mathrm{col}}}_{\mathrm{pl}} = N^{\mathrm{col}} - {N^{\mathrm{col}}}_{\mathrm{bg}}$, where ${N^{\mathrm{col}}}_{\mathrm{bg}}$ is the background (ambient) CO_2 column density. r_i is the range for spectrum i (or angle i as there was one average spectrum per angle). In the present case where the CO_2 LIDAR was placed on a tower and was scanning vertically, the angles were tilt angles and the range was computed as $r_i = \frac{h}{\sin\beta_i}$, where h is the height of the instrument over ground (height of the tower) and

$$\beta_i = \beta_S + i\Delta\beta. \tag{6}$$

To obtain u, the video tracking method described in detail in *Queißer et al.* [2016] was used.

3.4. Error Analysis

Using error propagation, for a given scanning angle i (for clarity this index is omitted in the following equations), the uncertainty of the column-averaged mixing ratio was calculated as

$$\left(\frac{\Delta X_{CO_2}}{X_{CO_2}}\right)^2 \approx \left(\frac{\Delta r}{r}\right)^2 + \left(\frac{\Delta N^{col}}{N^{col}}\right)^2. \tag{7}$$

The uncertainty of the CO_2 flux was evaluated using

$$\left(\frac{\Delta \Phi_{CO_2}}{\Phi_{CO_2}}\right)^2 \approx \left(\frac{\Delta u_{pl}}{u_{pl}}\right)^2 + \left(\frac{\sum_{Plume} r\Delta N^{col}{}_{pl}}{\sum_{Plume} rN^{col}{}_{pl}}\right)^2 + \left(\frac{\sum_{Plume} \Delta rN^{col}{}_{pl}}{\sum_{Plume} rN^{col}{}_{pl}}\right)^2, \tag{8}$$

where the range uncertainty Δr was estimated as (vertical scans only)

$$\left(\frac{\Delta r}{r}\right)^2 = \left(\frac{\Delta h}{h}\right)^2 + \left(\frac{\Delta \beta_{bias}}{\beta}\right)^2 + \left(\frac{\sigma_\beta}{\beta}\right)^2, \tag{9}$$

where Δh is the uncertainty of h and σ_β is the standard deviation of the tilt angle over the integration time per angle and is a measure of the steadiness (or linearity) of the tilt angle versus time. σ_β is significant as the scans were carried out manually. σ_β was retrieved from the asymptotic error of the linear fit of the recorded tilt angles over time. Since the stop angle did vary between scans, a bias $\Delta\beta_{bias}$ that takes this variation into account was added. The bias was estimated as follows. The angle at which the signal disappeared indicated the last useful data; since near 0 tilt angle the beam started to overshoot the trees at the opposite edge of the MV complex used as hard target. That means that the stop angle (last angle of data with signal-to-noise-ratio (SNR) $\geq$1) varied between -0.43 and $-0.27°$, adding a systematic error of $\Delta\beta_{bias} = 0.17°$.

For a given angle i, the measurement precision ΔN^{col} in equation (7) was calculated as described in *Queißer et al.* [2016]. In addition, it contains a variance accounting for the spectrum fitting error. This variance was retrieved as follows. The covariance matrix diagonal element corresponding to the best fit column density was, after taking the square root, scaled with the residual standard deviation of the fit (root-mean-square error). The uncertainty of the plume CO_2 column density in equation (8) was estimated as

$$\Delta N^{col}{}_{pl}{}^2 = \left(\Delta N^{col}\right)^2 + \sigma_{N^{col}{}_{bg}}{}^2, \tag{10}$$

where $\sigma_{N^{col}{}_{bg}}$ is the standard deviation of the mean ambient column density used as a bias estimate that contributes to the uncertainty of the plume CO_2 column density.

4. Results

4.1. Static Measurement of the Main Vent

The CO_2 LIDAR was placed on a platform about 200 m away from the center of the mud volcano to measure background ambient CO_2 (Figures 3a and 3b). The ambient CO_2 concentration was obtained by measuring CO_2 column densities at the edge of the mud volcano field using trees at 280 m distance as a topographic target (the instrument was not scanned). The resulting column density was found to be $N^{col}{}_{bg} = 2.74 \times 10^{24}$ m^{-2}, which corresponds to a background CO_2 gas concentration of 410 ppm (equation (3)) with a precision of $\sigma_{N^{col}{}_{bg}} = 20$ ppm. This is in agreement with expected background atmospheric concentrations.

Just before the measurements commenced, the onboard range finder LIDAR of the CO_2 LIDAR ceased to function due to humidity-related problems. This means that ranges could not be measured on site. As a solution, distances were retrieved in the postprocessing using Google Earth software and visual recognition of the topographic features that were used as backscattering sources.

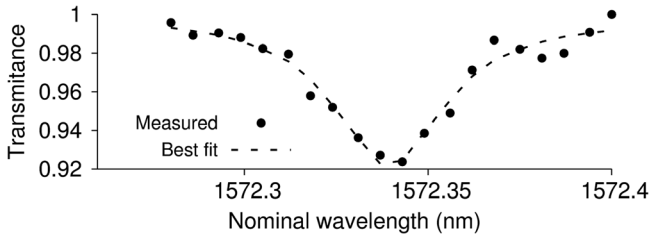

Figure 4. Spectrum acquired at Bledug Kuwu. Shown is the observed spectrum measured at 20 points (stack of 10 spectra, integration time 0.5 s) and the best fit transmittance.

The measurement strategy was focussed on measuring the gas flux produced by the main vent associated with bursting gas bubbles. The telescope was aligned such that its optical axis passed just above the height where ejected gas bubbles reached, i.e., ~ 1.2 m above ground. The time between the burst of the bubble (release of gas started) and the end of the ejection (bubble disappeared) was typically between 1 and 3 s (Figure 2). To resolve these events, but ensure adequate averaging, the integration time was set to 0.5 s, corresponding to 10 spectra (sweep rate 20 Hz) being averaged (stacked) per retrieved CO_2 concentration value (i.e., per scan angle). This integration time was used for all measurements. Figure 4 shows an example of a fitted spectrum used to compute CO_2 column densities or mixing ratios (equations (1)–(3)).

Every 2 to 20 s or so a gas bubble was produced by the mud volcano, ejecting gases, including water vapor and CO_2, as well as mud. As the absorption strength of the ejected fluids and gases strongly varied the beam was sometimes blocked by mud leading to poorly recovered spectra.

Using the approximate bubble diameter and the bubble frequency, a rough estimate of the expected CO_2 flux was obtained from

$$\Phi_{CO_2,\mathrm{bubble}} = f_{\mathrm{bubble}} \frac{\pi}{12} \frac{d^3 X_{CO_2,\mathrm{bubble}} M_{CO_2}}{V_m}, \tag{11}$$

where f_{bubble} depicts the bubble burst frequency, d the bubble diameter, $X_{CO_2,\mathrm{bubble}}$ the volume ratio of CO_2 inside the bubble, and V_m the molar volume of CO_2. Although temperatures at seeps at Bledug Kuwu were found to be between 28 and 30°C [*Satyana and Asnidar*, 2008], which is basically equal to the air temperature in that area, the presence of condensed water in the bursting bubbles indicated that the water was boiling and in the vapor phase with associated temperatures of at least 100°C when it reached the surface, in agreement with observations from *Mazzini et al.* [2012]. Flickering air in an ~ 2 m thick layer just above ground moreover indicated advection of hot air (> 30°C ambient temperature). Thus, to compute the molar volume of the gas inside the bubble just before bursting a temperature of 100°C was considered. Half-spherically shaped bubbles were assumed. The bubble diameter was obtained from calibrated video footage (the same as used for the plume speed retrieval) and was ranging from 1.9 to 3.4 m (average 2.5 m). The main vent has

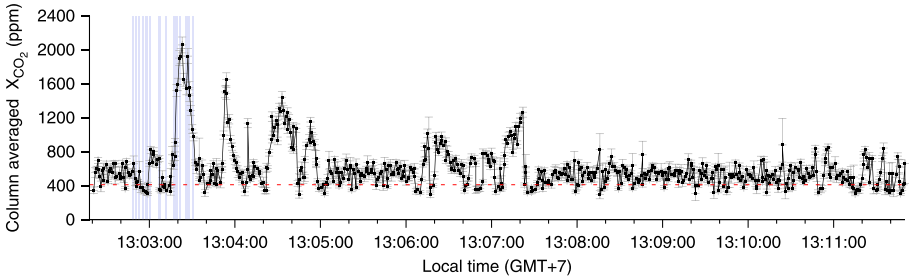

Figure 5. Static measurement of CO_2 from bursting bubbles. The graph shows path-averaged CO_2 concentrations from a static measurement performed on the 27 September 2016, aiming ~ 1.2 m above ground, just above the bubble explosions, which occurred ~200 m away from the CO_2 LIDAR. The instrument was located at position 1 (Figure 3a). The standard deviation of the mixing ratios (error bars) varies and is on average 31 ppm as derived with equation (7) using a range uncertainty of 20 m. There were bursts at least 8 times per minute. The blue bars indicate an example ensemble of visually confirmed bursts. The major peak at 13:03:20 is related to at least eight bubble explosions. The dotted line indicates the ambient CO_2 mixing ratio of 410 ppm.

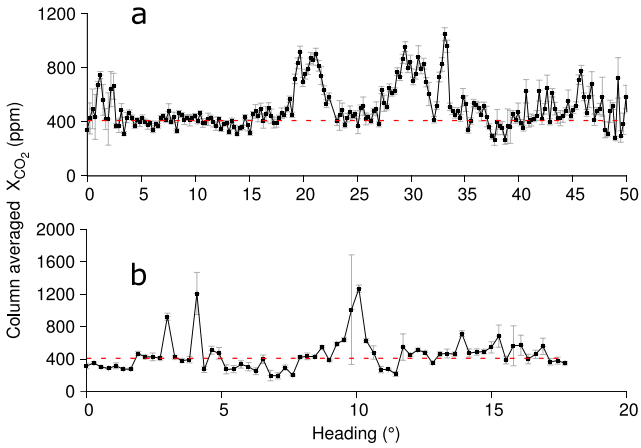

Figure 6. Horizontal scans of the main vent. (a) Scan from position 1 (Figure 3a). The high mixing ratios between 0 and 5° are likely related to the smaller vent, which was located west (to the right). Vent II is associated with 20° heading, while 30° coincides with the minor vent III. (b) Repeated scan from position 2, 40 m west of the first one with a narrower scanning range around the main vent, which is at 10°. The scanned sector corresponds to the sector between 10 and 29° in Figure 6a. The dotted line indicates the ambient CO_2 mixing ratio of 410 ppm.

been probed for 30 min out of which Figure 5 shows about 10 min. The time series suggests that the volume of ejected CO_2 was very variable, which was also indicated by the inconstant sizes of the bursting bubbles. Note that due to the limited field of view of the telescope (~ 0.6 m at bubble), which was passing the bubbles at ~1 m horizontal distance, and the dispersion of the CO_2, the bubble bursts identified visually do not necessarily coincide with the concentration peaks in Figure 5. However, as the larger concentration peaks likely correspond to larger bubbles (or clusters of fast occurring bubble bursts) they should coincide more than the smaller peaks. Automatically counting the peaks associated with CO_2 mixing ratios above average ambient mixing ratio plus twice the standard deviation ($2\sigma_{N^{col}_{bg}} = 40$ ppm) yielded a bubble burst frequency of 0.15 ± 0.04 s^{-1} or 9 ± 2.4 per minute. This is consistent with the estimated frequency of 7.5 explosions per minute from visual observation using the video footage. The bubbles were assumed to contain CO_2 only (i.e., bubble volume ratio $X_{CO_2,bubble} = 1$), yielding an upper limit flux of 0.9 ± 0.5 kg s^{-1}, just for the main vent, where for the uncertainty in bubble frequency and diameter is accounted for. Note that mainly due to the assumption of a single bubble bursting at a time and the semispherical shape assumption, this is a rough estimate merely yet providing an order of magnitude estimate of the CO_2 output of Bledug Kuwu.

4.2. Horizontal Scans

Since the gas plume advected horizontally, horizontal scanning of the plume was not adequate to retrieve the CO_2 flux, but it yielded valuable information about the shape and extension of the plume. Six consecutive scans were performed from two different instrument locations near each other (Figure 3a). Since the forest behind the mud volcano complex was used as a hard target, using Google Earth and the start and stop heading angle of the scans, the ranges could be reconstructed. This resulted in a larger range uncertainty, which was considered 20 m for all ranges (error assessment follows in discussion).

The TX/RX unit was rotated around the vertical axis with a velocity of 4 mrad/s (0.24°/s), corresponding to ~80 cm/s at the vent location, and was scanning the main vent (position 1, Figure 3a). The beam propagated ~1.5 m above ground, which means that it would pass undisturbed by most of the aerosols and mud expelled from the bubble bursts below it but would probe the gas expelled by the bubble. For some heading angles the laser may have been scattered not by the trees but by small water droplets or mud around the location of the vent. The resulting CO_2 mixing ratios are shown in Figure 6a. The sector associated with the circular zone of CO_2 propagating from the main vent outward corresponds to the angles between about 17° and 36°, associated with a lateral dimension of ~60 m. Interestingly, the minor vent (vent III, Figure 3a), which coincides with the twin peak near 30° has associated mixing ratios of magnitude equal to those near the main peak at 20° (associated with vent II). The oscillations between 41° and 50° are likely due to a changing hard target distance (such as tree lines at closer distance), which was difficult to discern without on-site range data. Mixing ratios far below the ambient level may indicate short ranges and that the beam was reflected by flying debris or dense condensed water vapor. The data were not omitted as the spectra were well recovered.

A repeated scan from a point 40 m close to the first instrument location (position 2, Figure 3a) showed a symmetrically decaying CO_2 concentration peak for the location of the main vent (10°, Figure 6b). As opposed to

the scan before in Figure 6a, the CO_2 mixing ratio for vent III (near 17°) is not very high. However, there are peaks near 3 and 4°, which correspond to the zone ~ 16 to 18 m west of the main vent (II). This area was in immediate reach of the concentric waves of gas emerging from the main vent, which have likely caused these peaks.

4.3. Vertical Scans and CO_2 Flux Retrieval

To obtain the CO_2 flux, the CO_2 concentration profile perpendicular to the propagation vector of the gas plume was needed. As the gas plume propagated horizontally (Movie S1) this required a vertical scan of the plume. Due to logistical constraints, the available equipment included neither tripod nor step motor. It was therefore decided to attempt a manual scan using the handrail of an observation tower as a mechanical support. This was an opportunity to assess whether the CO_2 LIDAR would provide useful data in hand-held operation. With the TX/RX unit placed on the handrail the instrument's height above ground was h = 5.3 m. The telescope's line of sight was intersecting the plume transport direction perpendicularly (Figures 3a and 3c). The scanning plane was located downwind, ~ 17 m west of the main vent (II). This means that the measured flux would correspond to the combined output of vents II and III (Figure 3a). Starting from a tilt angle of −4° (−0.07 rad), the TX/RX unit was manually moved upward so that the tilt angle was gradually increased until it reached 0. After a few trial runs the vertical scans were rather smooth, indicated by the linearity of the tilt angle with time. This is shown in Figure 3d for one of the scans along with the linear fit. The maximum asymptotic error $\sigma_\beta = 3 \times 10^{-3}$ °/s (0.05 mrad/s) of the linear fits of all scans was used as the tilt angle random error (standard deviation of the tilt angle, equation (9)). This corresponds to 8% of the scanning rate of 0.036°/s (0.6 mrad/s). The telescope was thus considered moving steadily. As before, spectra were acquired continuously at a rate of 20 Hz (50 ms sweep time per spectrum) and saved to disk each 0.5 s. Each tilt angle i was associated with a stack of 10 spectra (0.5 s integration time). Nine repetitions of the scan were recorded. The resulting CO_2 column densities and mixing ratios as a function of tilt angles and corresponding hard target ranges are shown in Figure 7. Despite the irregular degassing activity, both in terms of frequency and in terms of ejected volume (varying bubble size), column-averaged maximum mixing ratios usually peak around 1500 ppm, for some scans (e.g., Figures 7a, 7c, and 7d) much higher than that, up to at least 2400 ppm. The center of the mud volcano mouth was located at a range of 230 m. Although these peaks fluctuate from scan to scan, the highest mixing ratios are predominantly found near that range, between ~130 and ~300 m. This range is consistent with the observed maximum water vapor plume extent, indicating the minimum radial extension of the CO_2 plume.

The prevailing transport direction of the plume was toward northwest, explaining a possibly a concentric distribution of the plume. This may have led to higher CO_2 concentrations toward north, that is, toward the instrument position. It is also important to note that the X_{CO_2}represent total column-averaged mixing ratios, which include ambient CO_2. So with increasing range the relative contribution of the plume CO_2 to X_{CO_2}decreases.

There is a reoccurring peak near 120 m. An explanation could be that due to the reoccurrence of bubble explosions, peaks farther away from the vent stemmed from previous bubble explosions seconds before. On the video (Movie S1) this is revealed by concentric waves of condensed water vapor overriding each other as they propagate along the ground. The same was probably true for the CO_2.

The column density remains high after the bubble center (after ~270 m). Note that the range increased nonlinearly with tilt angle, which means that the associated column densities correspond to much lower CO_2 mixing ratios (Figure 7). Assuming an air density of ~1.2 kg m^{-3}, even at a gas temperature of 100°C upon exiting the vent, the CO_2 density would still have been higher than the air density. The CO_2 therefore would have still not been buoyant but held down by gravity. However, the instrument might well have been probing plume CO_2 at ranges >400 m, due to the quasi-steady supply by the vents and the fact that for a given vertical scanning angle the laser beam height above ground geometrically decreased (Figure 3c). For instance, for the given range of r = 660 m, the height above ground for 230 m, 300 m, and 400 m away from the instrument was 4.7 m, 3.3 m, and 2.5 m, respectively. This is of the order of the bubble diameter.

The vertical plume velocity component was zero. The horizontal transport speed was remarkably constant and associated with a constant progression of the plume fronts emanating from the center of the puddle (the bubble burst zone), which were tracked. A single value for the plume speed resulting from the

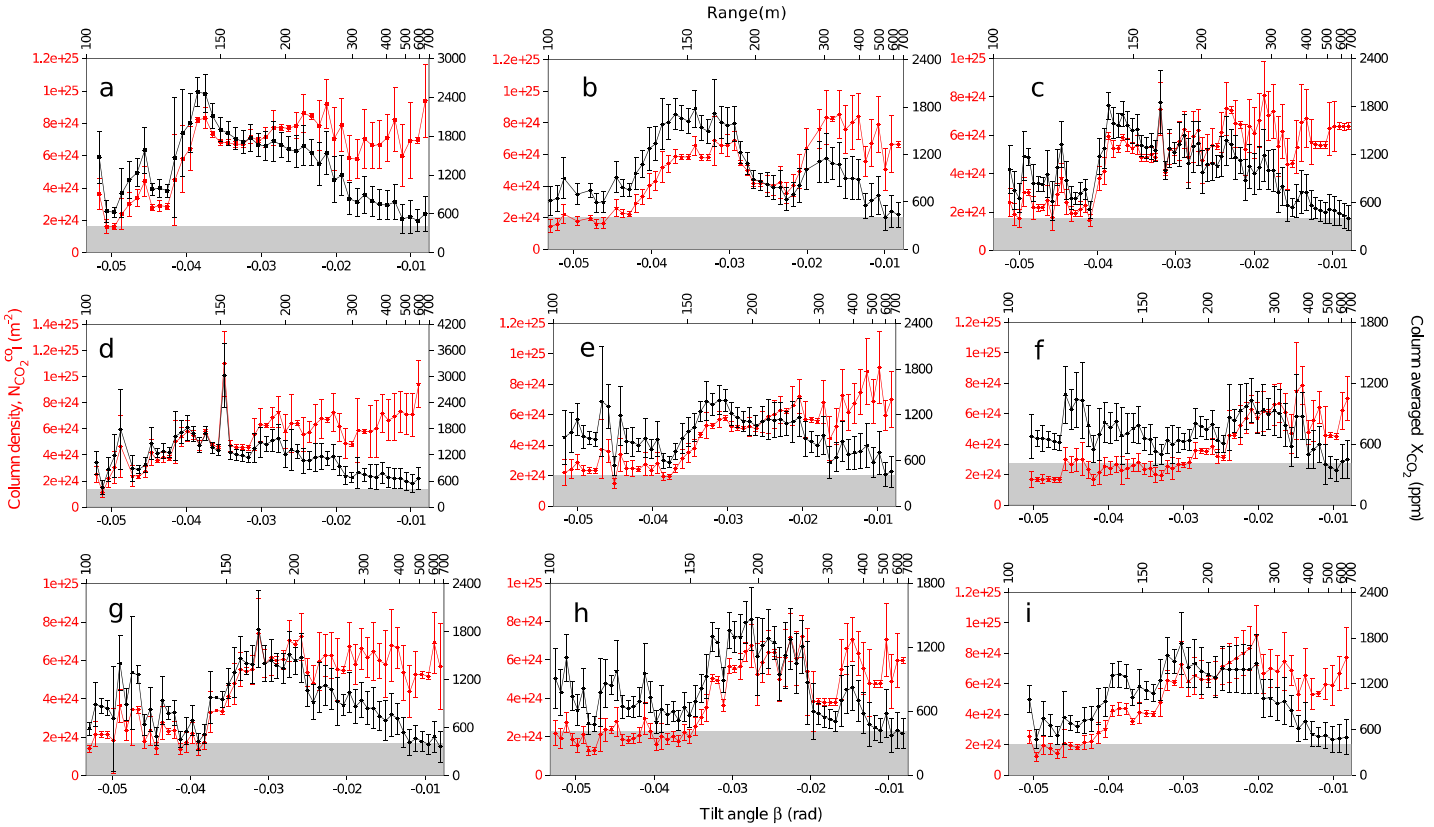

Figure 7. (a–i) CO_2 column densities and converted mixing ratios for the vertical scans. The scans were acquired on the 28 September 2016 between 7 h11 and 7 h47 A.M. local time. They are presented in the order they were carried out. Each scan took ~1 min and was spanning the complete extension of the mud volcano field. The column densities resulting from these scans were used to compute the CO_2 fluxes in Table 1. The grey shaded area depicts the ambient CO_2 mixing ratio of 410 ppm.

average of tracks of 25 different fronts was retrieved. The transport speeds of the different tracks ranged from a minimum of 0.36 m s^{-1} to a maximum of 1.2 m s^{-1} with a mean of 0.69 m s^{-1} and standard deviation of 0.23 m s^{-1}.

For each scan the CO_2 flux was computed using equation (4) and the uncertainties using equation (8). The results are presented in Table 1. The average flux of all nine scans is 1.4 ± 0.8 kg s^{-1} or 117 ± 68 t d or 43 kt yr^{-1}. It agrees with the flux estimated for vent II of 0.9 ± 0.5 kg s^{-1} using equation (11). Note that 1.4 kg s^{-1} accounts for both vents II and III. However, the video footage revealed that bubble explosions at vent III were at least 20 times less frequent and the bubble diameter is about 3 times smaller, implying that, given the error bars, 1.4 kg s^{-1} represents the flux of the main vent II to first order.

Table 1. CO_2 Fluxes From the Vertical Scans[a]

Scan	Flux Φ_{CO_2} (kg s^{-1})
a	2.07 ± 1.01
b	1.49 ± 0.91
c	1.37 ± 0.69
d	1.86 ± 1.36
e	1.42 ± 0.78
f	0.89 ± 0.65
g	0.69 ± 0.32
h	0.90 ± 0.56
i	1.55 ± 0.81

[a]The fluxes were obtained by integrating over the whole profile, starting from a range of 100 m. The scans are identified with the same letter as in Figure 7. The horizontal transport speed was found to be u= 0.69 ± 0.23 m s^{-1}. The mean of all nine flux values is 1.4 ± 0.8 kg s^{-1} (117 ± 68 t d^{-1}).

5. Discussion

5.1. Uncertainties

The SNR contributed an uncertainty of ~2% of the column density, whereas the fit contribution varied

between 4% of the column density for a smooth spectrum and 20% for a noisy spectrum. The resulting relative uncertainty of N^{col}_{pl} was between 4% and 30%, mainly depending on the quality of the fit, which in some cases dominated the uncertainty.

For the vertical scans, the fit error alone contributed an uncertainty of the CO_2 flux of 44% on average. Highest fit errors are produced from relatively noisy spectra collected in the near and the very far range measurements. For the shorter ranges ($<$ 150 m) speckle noise contributes significantly [*Queißer et al.*, 2016]. For the longer ranges the angle increment $\Delta\beta$ produced a field of view, which included a wide topographic target range (e.g., ~0.5 m near 0.07 rad versus ~25 m near 0.01 rad). Along with bushes and trees that were found near the edge of the mud volcano this significantly altered the target reflectivity during each sweep, producing an additional interfering signal in the transmittance spectra. Furthermore, it was raining during the vertical scans (see Movie S1). Other than an increased light extinction and thus noisy spectra, particularly for the longer ranges, this gave rise to an angle-dependent noise contribution [*Roy and Bissonette*, 2001]. Water puddles at places produced reflectivity patterns of small-scale (~m) heterogeneity (mud versus water) that could have introduced noise in the spectra, especially those collected at longer range.

One should also mention that the relatively short integration time of 0.5 s (stack of 10 subsequent spectra) was contributing to a rather high fitting error. On the other hand, a short integration time was needed to account for the plume dynamics, so that the "frozen plume" assumption holds.

As far as the range error is concerned, for the horizontal scans and the static measurement, the lack of range data entailed an increase in range uncertainty from $<$1 m (with the range finder) to 20 m. For the vertical scans the range uncertainty is accounted for by the angle uncertainty (equation (9)). For the horizontal scans the increase in range uncertainty corresponded to an increase in uncertainty of the CO_2 mixing ratios of up to 40%, depending on the range and relative error of the column density (equation (7)). For the vertical scans, the lack of the range finder entailed an increase in flux uncertainty between 5% (scan d) and 10% (scan a).

Temperature and pressure uncertainties cause an uncertainty in differential absorption cross section, which contributes to the error of the CO_2 column density. The pressure was steady. Assuming a realistic temperature uncertainty of 2 K, the error of N^{col}_{pl} due to temperature uncertainty was only 0.3% and hence was neglected.

5.2. Context of the Bledug Kuwu CO_2 Emissions

Given that the Bledug Kuwu is a local tourist destination and visitors approach the main vent as close as 20 m (based on our observation), it is beneficial to assess CO_2 emissions from a health and safety perspective. Measured CO_2 mixing ratios in the vicinity of the main vent (~ 80 m around the crater) were found to reach up to 2400 ppm, that is, averaged over the path length (Figure 7). In terms of personal health and safety this value is well below the threshold of 5000 ppm per 8 h exposure [*EH40/2005*, 2011]. A high-risk column-averaged concentration ($>$ 15,000 ppm over 15 min) would only be caused if there was an area of a few meter size with nearly pure CO_2, for instance, a 2.5 m path (to take the average size of a bubble) consisting of 90% CO_2.

The retrieved CO_2 flux of 117 t d^{-1} is in line with that measured at the LUSI mud volcano, also located in the Kendeng Basin, 180 km east of Bledug Kuwu (Figure 1), which was reported to be between 35 and 160 t d^{-1} [*Vanderkluysen et al.*, 2014]. This order of magnitude of CO_2 flux compares with the lower end of volcanic emission rates, such as Vulcano, Italy [*Gerlach et al.*, 1997], and, by itself, is dwarfed by the anthropogenic carbon emissions in Indonesia, which are of the order of 274 kt d^{-1} (http://cdiac.ornl.gov/trends/emis/ido.html). For a comparable emission rate, hundreds of Bledug Kuwu-like emitters would be necessary.

It is not straightforward to provide an estimate of the total CO_2 flux of Javanese back-arc MV since there is no comprehensive summary of all Javanese MV, and the number of MV in the literature is inconsistent between different sources [*Satyana and Asnydar*, 2008; *Guntoro*, 2011]. Moreover, MV may sometimes not be defined as such. For instance, Kamojang, located in Western Java, is characterized as a geothermal field with mud pods [*Setijadji*, 2010]. In addition, the CO_2 content of the gas emitted by Javanese MV generally varies strongly. For example, the molecular composition observed for gas emitted by different MV near LUSI varied between $<$1% and 99 vol % of CO_2 [*Mazzini et al.*, 2012]. Nevertheless, encouraged by the similarity of the CO_2 flux between LUSI and Bledug Kuwu, we attempt at least an order of magnitude estimation. A

Table 2. CO_2 Volume Fraction in Gas Released From 28 Javanese Mud Volcanoes, Using Literature Values[a]

Name of Mud Volcano	Reference	CO_2 Fraction in Vol %
	Central Java and East Java	
Sidoarjo (LUSI)	*Mazzini et al.* [2012]	1 to 90
Gunung Anyar	*Mazzini et al.* [2012]	18
Kalang Anyar	*Mazzini et al.* [2012]	3 to 9
Gunung Sening	*Mazzini et al.* [2012]	0.4
Pulungan	*Mazzini et al.* [2012]	4
Pangangson	*Mazzini et al.* [2012]	6 to 7
Kepulungan	*Mazzini et al.* [2012]	ND
Gunung Bulag	*Mazzini et al.* [2012]	2.5
Songgoriti	*Mazzini et al.* [2012]	99
Cangar	*Mazzini et al.* [2012]	ND
Pacet	*Mazzini et al.* [2012]	ND
Gresik	*Guntoro* [2011]	ND
Dawar Andong	*Guntoro* [2011]	ND
Denanyar	*Guntoro* [2011]	ND
Probolinggo	*Guntoro* [2011]	ND
Socah (Madura Island)	*Satyana and Asnidar* [2008]	ND
Bledug Kuwu	This work	≥16
Cangring Bledug	*Istadi et al.* [2012]	ND
Bledug Banjarsari	*Istadi et al.* [2012]	ND
Bledug Crewek	*Istadi et al.* [2012]	ND
Medang Kamolan	*Istadi et al.* [2012]	ND
Sangiran	*McLachlan-Karr et al.* [2009]	ND
Tuban	*McLachlan-Karr et al.* [2009]	ND
	West Java	
Kamojang	*Setijadji* [2010]	ND
4 near Ciuyah (names unknown)	*Satyana and Asnidar* [2008]	ND

[a]For values by *Mazzini et al.* [2012] the water volume fraction was not considered.

conservative number of Java's subaerial MV is 28, of which 23 are located in the eastern half of Java (Table 2). The highest MV density is found in the province of East Java. Extrapolating the fluxes of LUSI and Bledug Kuwu on all Javanese MV yields an order of magnitude CO_2 flux of 3 kt d^{-1}. Mount Merapi's CO_2 flux is ~600 t d^{-1} (vented + diffuse slope degassing) during quiescent periods [*Toutain et al.*, 2009]. Extrapolating this value over the 20 or so, actively degassing Javanese arc volcanoes yields a ballpark figure of ~12 kt d^{-1} for the CO_2 emitted by Javenese arc volcanism. This implies that the extrapolated CO_2 flux from Javanese back-arc MV accounts for 3/12 or 25% of the CO_2 flux from arc volcanism in Java. In general, the back-arc diffuse degassing of magmatic carbon is estimated to account for roughly 26% of the carbon flux of arc volcanoes at subduction zones [*Kelemen and Manning*, 2015]. If assumed that back-arc outgassing of magmatic carbon occurs mainly via CO_2, this suggests that the extrapolated mass of carbon emitted by Javanese MV is comparable with the mass emitted by back-arc diffuse outgassing (not emitted by arc volcanoes). The question arises whether some of the CO_2 emitted by the back-arc MV is of magmatic origin.

5.3. Origin of the CO_2 Emitted at Bledug Kuwu

Here we examine possible sources of CO_2 emitted at Bledug Kuwu. We highlight that our data do not permit an unequivocal conclusion with regard to CO_2 sources; however, the key mechanisms can be examined and compared. A major constituent of the gas emitted at Bledug Kuwu is water vapor. This is apparent from visual observation of the bubbles, which upon bursting produce abundant condensed water vapor fumes (Figure 2), suggesting decompression of water vapor to drive the explosions. The fact that one can observe a point source of expelled CO_2 and since the CO_2 is expelled along with water suggests that CO_2 was originally dissolved in water in the saturated zone. In this sense the eruption can be modeled and characterized as a geyser. We therefore adopt the conceptual model of a geyser [*Lu et al.*, 2005], which consists of a conduit between the surface and an underground chamber where liquid is heated, decreases in density, and ascends up the conduit to the surface, boiling during ascent. Such a conduit is consistent with the general

understanding of mud volcanoes as soft matter migrating toward the surface through low-pressure channels in the form of liquid mud diapirs and gas.

The eruption mode at Bledug Kuwu is similar to LUSI [*Mazzini et al*., 2012] and can be characterized by a churn flow regime, that is, a multiphase gas flow with interacting bubbles upon boiling [*Vanderkluysen et al*., 2014]. CO_2 is considered to have been dissolved in the aquifer water before exsolving during ascent or in a shallow storage zone. It is assumed that all water evaporates completely upon the bubble explosion, so that all CO_2 separates from the water. The molar ratio between water vapor and CO_2 observed after the bubble explosion therefore represents, to first order, the molar ratio in the subsurface when CO_2 was dissolved in the water.

In addition to water vapor and CO_2, mud volcanoes may emit methane and other gases. Since our CO_2 LIDAR measured CO_2 only, trace gas compositions of the bubble could not be analyzed. *Mazzini et al*. [2012] reported, however, that the gas expelled at Bledug Kuwu is dominated by CO_2. This is in line with *Satyana and Asnidar* [2008], who stated that the emitted gases at Bledug Kuwu have been reported to be mainly H_2O and CO_2 with traces of H_2S. We therefore assume that the methane content of the gases expelled at Bledug Kuwu is present in low amounts and it is not considered in our mass balance calculation. The ejected liquid is thus treated as a two-phase mixture of muddy water and a gas phase of water vapor and CO_2. Using equation (11) and plugging in the flux obtained with the CO_2 LIDAR and solving for $X_{CO_2,bubble}$ yields a CO_2 volume fraction of 1. The inputs for equation (11) have significant uncertainties. Considering the maximum error caused by the uncertainties of the flux, bubble diameter and bubble frequency yield that a minimum fraction of 0.16 of the volume of the ejected bubbles at the main vent at Bledug Kuwu was occupied by pure CO_2.

Considering that both CO_2 and water vapor are at the same temperature and pressure implies that their molar ratio is at least 16:84 or 0.19. For simplicity we consider that all the CO_2 is dissolved in brine up to a certain depth (and pressure). Then Henry's law can be employed together with the molar ratio of H_2O vapor and CO_2 gas to estimate the subsurface pressure at which CO_2 exsolved from the brine. A gas temperature of 100°C upon piercing the surface is considered here. Considering a water density of 1030 kg/m^3 using the relationship of *Crovetto* [1991], the Henry volatility constant is retrieved as 96 L atm mol^{-1}. Neglecting the fact that the salt content in the brine decreases solubility and that the molar ratio of 0.19 of CO_2 is a lower limit and considering the geothermal gradient with temperatures at the Kendang base likely higher than 300°C [*Nurhandoko et al*., 2016; *Putra et al*., 2016] yields a pressure of at least ~106 MPa or a minimum dissolution depth of 10 km.

The large negative gravity anomaly of the Kendeng zone [*Smyth et al*., 2008] indicates a deep sedimentary basin with an average sediment thickness of ~6 km that may reach down to 10 km below where Bledug Kuwu is located [*Untung and Sato*, 1978; *Waltham et al*., 2008]. It is therefore possible that the CO_2 observed at Bledug Kuwu originated from the basement of the Kendeng Basin or from below.

Mazzini et al. [2012] noted that samples taken at different vents at mud volcano sites may exhibit different isotopic signatures, suggesting mixed sources of CO_2. For instance, at LUSI three samples suggested volcanic origin of the CO_2, while the majority of samples taken at LUSI pointed toward an organic origin of CO_2. *Setijadji* [2010] considered Bledug Kuwu not being linked to a volcanic center. This is supported by the reported $\delta^{13}C$ of the CO_2 of $-18.8‰$ measured at Bledug Kuwu, which indicates an organic origin of the CO_2, such as from decarboxylation of kerogen [*Mazzini et al*., 2012]. Potential CO_2 source rocks include the kerogene bearing, 4400 m deep Ngimbang rock formation [*Mazzini et al*., 2012], and the deeper Paleocene pre-Ngimbang formation [*Satyana and Purwaningsih*, 2003; *Wiloso et al*., 2009]. The corresponding depth region near the base of the Kendeng Basin (Eocene) is, however, poorly studied and leaves room for alternative sources. As it is located in a setting favorable for hydrocarbon production [*Satyana and Purwaningsih*, 2003; *Wiloso et al*., 2009], it is remarkable that Bledug Kuwu is dominated by emission of CO_2 rather than methane. This advocates the prospect that at least to some extent the CO_2 may originate from oxidation of methane via reduction of pyrite and SO_4 [*Seewald et al*., 1994; *Mazzini et al*., 2012].

Java is located in a tectonically active region with extensive deformation observed throughout the arc. Thrusting once displaced some of the early Cenozoic volcanic arc to which Mount Muria belongs northward (Figure 1). Central Java hosts a series of these northward directed thrusts [*Clements et al*., 2009]. Bledug Kuwu and other MV of Central Java are mainly located along the NE-SW Kendeng Fault, which is dominated by

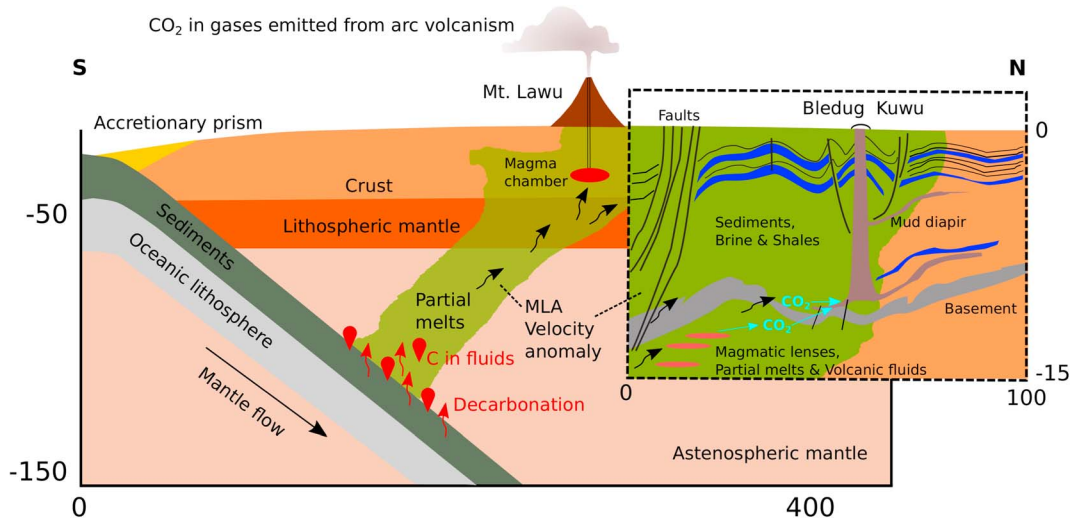

Figure 8. Conceptual model of the subduction zone beneath Bledug Kuwu MV in Central Java and blowup of the Kendeng Basin hosting Bledug Kuwu MV. The length scale is in kilometers. Kendeng Basin faults have been compiled after *Waltham et al.* [2008]. Curved arrows indicate upward migrating volcanic fluids and partial melts within the Merapi Lamu velocity anomaly (MLA) [after *Wagner et al.*, 2007; *Koulakov et al.*, 2009] containing disolved CO_2 from decarbonation. The Kendeng Basin contains brine-saturated sediments and shales (e.g., Wonocolo and Ngimbang). Beneath Bledug Kuwu an upward convex mud diapir (not to scale) is fed by brine-saturated sediment layers. As they cool, partial melts and volcanic liquids pond beneath the basin basement or enter the basin via faults. Between 15 and 11 km depth CO_2 could exolve from the partial melt, potentially migrate through faults, and dissolve into sediment brine, which moves upward. As depth decreases the mud diapir forms. With pressure decreasing, close to the surface, the uprising muddy brine boils with large bubbles piercing the surface, releasing water vapor and CO_2. Not shown are other potential CO_2 source mechanisms involved, such as contact metamorphism, oxydation of methane, or decarboxylation.

thrusting. Some of the folds and thrusts are torn by strike-slip faults oriented obliquely to the trend of the thrust fault and fold axis. Many of the mud volcanoes are found in the intersection of these structures. The association of mud volcanoes with these structures suggests that faulting and folding are the chief control of MV emplacement in the region [*Setijadji*, 2010; *Roberts et al.*, 2011]. These faults on Java are potentially acting as a pathway for hydrothermal fluids to the surface [*Mazzini et al.*, 2014].

It is peculiar that some of the MV are methane dominated and associated with colder temperatures $<$100°C [*Mazzini et al.*, 2012], while the CO_2-dominated MV emissions are hot, such as Bledug Kuwu and LUSI. A CO_2 dissolution depth of 10 km or more below Bledug Kuwu would likely be in reach of rising volcanic fluids. This raises the possibility that in the Bledug Kuwu case an igneous intrusion or magma storage zone may be both a source of heat and CO_2, leaking into the sedimentary basin through fractures. *Mazzini et al.* [2012] postulated the occurrence of a magma chamber at 6 km depth that may interact with sediments at the base of the Kendeng Basin.

Earthquake attenuation tomography is capable of outlining zones of high attenuation and seismic velocity anomaly, such as caused by magma. *Bohm et al.* [2013] performed seismic attenuation tomography using arrivals from earthquakes down to 200 km depth below Central Java. The model resolution of 15 km vertical and 30 km horizontal was too coarse to help differentiate between zones of high temperature, such as magma intrusions, and the water-saturated sediments of the Kendeng Basin, which also strongly attenuate seismic energy. Their models suggested fluid-saturated sediments down to 15 km depth at the Kendeng Basin. The findings, however, did not indicate a large-scale, high attenuation channel between partial melt zones of the volcanic centers ($<$15 km to 30 km depth) and the Kendeng Basin, which would imply pathways for magma, partial melts or CO_2 rich fluids.

In line with the high attenuation at the location of the Kendeng Basin, passive seismic velocity tomography performed by *Koulakov et al.* [2007 and 2009] and active seismic tomography carried out by *Wagner et al.* [2007] indicated the occurrence of a strong low-velocity anomaly (Merapi Lawu anomaly, MLA) north of the volcanic arc, reaching at least until Mount Lawu to the east (Figure 1). They explained the anomaly by

thick sediments, saturated with fluids and gases, and also magma and partial melts. Unlike the seismic attenuation model of *Bohm et al*. [2013], their velocity models suggested the MLA to continue until the subducting slab, that is, beneath the volcanic arc at ~120 km depth. Their model therefore indicates a potential pathway of magmatic CO_2 into the Kendeng Basin. It is possible that melts or partial melts reach the base of the Kendeng Basin where their temperature is lowered by relatively cold sediments of the Kendeng Basin, which are sealing off the hot volcanic fluids [*Koulakov et al*., 2007] or allow small amounts of volcanic fluids to penetrate the sedimentary layers near the basement base [*Wagner et al*., 2007; *Koulakov et al*., 2009]. *Koulakov et al*. [2009] furthermore suggested the possible presence of magmatic lenses reaching up to 11 km depth. In summary, based on seismic tomography, magmatic CO_2 could indeed reach the Kendeng Basin, be dissolved in brine, and eventually be expelled via mud volcanoes. Figure 8 illustrates this possibility by showing a potential pathway of magmatic CO_2 into the mud diaper of Bledug Kuwu. But owing to the limited resolution of ~15 km of the data, this remains a possibility rather than a fact.

In the light of a mixed origin of the CO_2 not all of the CO_2 reaching the surface is dissolved below 10 km. More likely, an unknown amount of magmatic CO_2, corresponding to a fraction of the measured 1.4 kg s^{-1}, is dissolved at depths of 10 km or below, while biogenic and thermogenic CO_2, dissolve at shallower depths, for instance, at ~4000 m within the Ngimbang rock formation. This means that the CO_2/H_2O molar ratio at a given depth and the nucleation depth of CO_2 bubbles are unknown.

Given all evidence combined, it is likely that the CO_2 emitted at Bledug Kuwu is a mixture of thermogenic or biogenic CO_2 and magmatic CO_2. Volcanic fluids and melts could also catalyze CO_2 production. As speculated for the alike LUSI [*Mazzini et al*., 2012], rocks near the base of the Kendeng Basin could be affected by intruding magma or partial melts and, due to the heat supply, promote thermogenic production of CO_2 from the limestone basement of the basin through contact metamorphism.

Although geological, geophysical, and geochemical mapping has been done for Central Java, at the current stage more confining evidence, particularly of the geochemical sort, is necessary to exclude that CO_2 expelled by Bledug Kuwu and other MV in Central Java is not of volcanic origin. A powerful yet inexpensive approach compared with, for instance, high-resolution seismic could be to measure $CO_2/^3He$ ratios.

6. Conclusions

Studying the quantity and origin of CO_2 emitted by back-arc mud volcanoes is important to correctly model the thermodynamics and geochemistry of arc volcanoes and to constrain their role in the carbon budget and hence the global geochemical carbon cycle. Using remote sensing laser absorption spectroscopy, an average CO_2 flux of 1.4 kg s^{-1} or 117 t d^{-1} (43 kt yr^{-1}) was found at Bledug Kuwu mud volcano. The flux stems from two of three identified main vents and thus represents a lower limit.

The gas flow was characterized as a two-phase slug flow of brine and CO_2 with CO_2 dissolving at depths that may reach below 10 km. Geochemical and geological evidence suggest the CO_2 observed at Bledug Kuwu to be of biogenic or thermogenic origin. Seismic tomography, the tectonic setting, and the depth of the CO_2 origin, on the other hand, favor at least a partly magmatic origin of the CO_2. A more focused effort, such as noble gas tracing, is needed to clarify the origin of the CO_2 released at Bledug Kuwu, in particular the contribution of magmatic CO_2 if there is any.

This study not only demonstrated the merit of a man-portable active remote sensing instrument for probing natural gas releases but also showed feasibility of a hand-held scan of a gas release to obtain the gas flux, enabling efficient bottom-up estimation of CO_2 fluxes. To our knowledge, this was the first time the CO_2 flux of a mud volcano was measured using ground-based remote sensing.

Acknowledgments
The research leading to these results has received funding from the European Research Council under the European Union's Seventh Framework Programme (FP/2007-2013)/ERC Grant Agreement 279802. We thank undergraduate students of the Universitas Gadjah Mada: Muhammad Arba Azzaman, Rini Fahmita, and Satrio Widianto for their assistance during the field work. We thank two anonymous reviewers and the Associate Editor Luca Caricchi, who helped improve the manuscript. The data acquired at Bledug Kuwu are stored at the University of Manchester's research data repository and may be requested by contacting the corresponding author or mike.burton@manchester.ac.uk.

References

Aiuppa, A., L. Fiorani, S. Santoro, S. Parracino, M. Nuvoli, G. Chiodini, C. Minopoli, and G. Tamburello (2015), New ground-based lidar enables volcanic CO_2 flux measurements, *Sci. Rep.*, *5*, 13614, doi:10.1038/srep13614.

Abshire, J. B., H. Riris, G. R. Allan, C. J. Weaver, J. Mao, X. Sun, W. E. Hasselbrack, S. Randoph Kawa, and S. Biraud (2010), Pulsed airborne lidar measurements of atmospheric CO_2 column absorption, *Tellus B*, *62B*, 770–783.

Barber, A. J., S. Tjokrosapoetro, and T. R. Charlton (1986), Mud volcanoes, shale diapirs, wrench faults, and melanges in accretionary complexes, eastern Indonesia, *AAPG Bulletin*, *70*, 1729–1741.

Bohm, M., C. Haberland, and G. Asch (2013), Imaging fluid related subduction processes beneath Central Java (Indonesia) using seismic attenuation tomography, *Tectonophysics*, *590*, 175–188, doi:10.1016/j.tecto.2013.01.021.

Brantley, S. L., and K. W. Koepenick (1995), Measured carbon dioxide emissions from Oldoinyo Lengai and the skewed distribution of passive volcanic fluxes, *Geology*, *23*, 933–936.

Burton, M., G. Sawyer, and D. Granieri (2013), Deep carbon emissions from volcanoes, *Rev. Mineral. Geochem.*, *75*, 323–354.

Burton, M. R., C. Oppenheimer, L. A. Horrocks, and P. W. Francis (2000), Remote sensing of CO_2 and H_2O emission rates from Masaya volcano, Nicaragua, *Geology*, *28*(10), 915–918.

Clements, B., R. Hall, H. R. Smyth, and M. A. Cottham (2009), Thrusting of a volcanic arc: A new structural model for Java, *Pet. Geosci.*, *15*, 159–174, doi:10.1144/1354-079309-831.

Connolly, J. A. D. (2005), Computation of phase equilibria by linear programming: A tool for geodynamic modeling and its application to subduction zone decarbonation, *Earth Planet. Sci. Lett.*, *236*, 524–541.

Crovetto, R. (1991), Evaluation of solubility data of the system CO_2-H_2O from 273 K to the critical point of water, *J. Phys. Ref. Data*, *20*(3), 575–589.

Dimitrov, L. I. (2002), Mud volcanoes—The most important pathway for degassing deeply buried sediments, *Earth Sci. Rev.*, *59*, 49–76.

Duffell, H., C. Oppenheimer, and M. Burton (2001), Volcanic gas emission rates measured by solar occultation spectroscopy, *Geophys. Res. Lett.*, *28*(16), 3131–3134, doi:10.1029/2000GL012425.

EH40/2005 (2011), Workplace exposure limits, HSE books, ISBN 9780717664467. [Availabe atwww.hse.gov.uk/pubns/priced/eh40.pdf.]

Etiope, G., T. Fridriksson, F. Italiano, W. Winiwarter, and J. Theloke (2007), Natural emissions of methane from geothermal and volcanic sources in Europe, *J. Volcanol. Geotherm. Res.*, *165*, 76–86.

Füri, E., D. R. Hilton, M. D. Tryon, K. M. Brown, G. M. McMurtry, W. Brückmann, and C. G. Wheat (2010), Carbon release from submarine seeps at the Costa Rica fore arc: Implications for the volatile cycle at the Central America convergent margin, *Geochem. Geophys. Geosyst.*, *11*, Q04S21, doi:10.1029/2009GC002810.

Galle, B., C. Oppenheimer, A. Geyer, A. L. McGonigle, M. Edmonds, and L. A. Horrocks (2003), A miniaturised ultraviolet spectrometer for remote sensing of SO_2 fluxes: A new tool for volcano surveillance, *J. Volcanol. Geotherm. Res.*, *119*, 241–254.

Gerlach, T. M., H. Delgado, K. A. McGee, M. P. Doukas, J. J. Venegas, and L. Cárdenas (1997), Application of the LI-COR CO_2 analyzer to volcanic plumes: A case study, volcán Popocatépetl, Mexico, June 7 and 10, 1995, *J. Geophys. Res.*, *102*, 8005–8019, doi:10.1029/96JB03887.

Gerlach, T. M., K. A. McGee, A. J. Sutton, and T. Elias (1998), Rates of volcanic CO_2 degassing from airborne determinations of SO_2 emission rates and plume CO_2/SO_2: Test study at Pu'u 'O'o Cone, Kilauea volcano, Hawaii, *Geophys. Res. Lett.*, *25*, 2675–2678.

Gerlach, T. M., K. A. McGee, T. Elias, A. J. Sutton, and M. P. Doukas (2002), Carbon dioxide emission rate of Kīlauea Volcano: Implications for primary magma and the summit reservoir, *J. Geophys. Res.*, *107*, 2189, doi:10.1029/2001JB000407.

Giammanco, S., F. Parello, B. Gambardella, R. Schifano, S. Pizzullo, and G. Galante (2007), Focused and diffuse effluxes of CO_2 from mud volcanoes and mofettes south of Mt. Etna (Italy), *J. Volcanol. Geotherm. Res.*, *165*, 46–63, doi:10.1016/j.jvolgeores.2007.04.010.

Gorman, P. J., D. M. Kerrick, and J. A. D. Connolly (2006), Modeling open system metamorphic decarbonation of subducting slabs, *Geochem. Geophys. Geosyst.*, *7*, Q04007, doi:10.1029/2005GC001125.

Guntoro, A. (2011), Understanding the origin of Sidarjo mud volcano in relation to longevity estimation based on regional study and seismic interpretation, Trisakti University May 26, 2011. [Available at http://www.hsf.humanitus.org/media/14190/Presentation-5th-Symposium-25mei2011.pdf, accessed 12/12/2016.]

Hall, R., and H. R. Smyth (2008), Cenozoic arc processes in Indonesia: Identification of the key influences on the stratigraphic record in active volcanic arcs, in *Formation and Applications of the Sedimentary Record in Arc Collision Zones*: *Geol. Soc. Am. Spec. Pap.*, 436, A. E. Draut, P. D. Clift, and D. W. Scholl, pp. 27–54, Geol. Soc. Am., Denver, doi: 10.1130/2008.2436(03).

Hernández, P. A., et al. (2015), Contribution of CO_2 and H_2S emitted to the atmosphere by plume and diffuse degassing from volcanoes: The Etna volcano case study, *Surv. Geophys.*, *36*, 327–349, doi:10.1007/s10712-015-9321-7.

Istadi, B. P., H. T. Wibowo, E. Sunardi, H. Soffian, and N. Sawol (2012), Mud volcano and its evolution, earth sciences, edited by Dr. Imran Ahmad Dar, doi:10.5772/24944. [Available from: http://www.intechopen.com/books/earth-sciences/mud-volcano-and-its-evolution.]

Kelemen, P. B., and C. E. Manning (2015), Reevaluating carbon fluxes in subduction zones, what goes down, mostly comes up, *Proc. Natl. Acad. Sci. U.S.A.*, *112*, 3997–4006, doi:10.1073/pnas.1507889112.

Kerrick, D. M., and J. A. D. Connolly (2001), Metamorphic devolatilization of subducted marine sediments and the transport of volatiles into the Earth's mantle, *Nature*, *411*, 293–296.

Kopf, A. (2002), Significance of mud volcanism, *Rev. Geophys.*, *40*, 1005, doi:10.1029/2000RG000093.

Koulakov, I., et al. (2007), *P* and *S* velocity structure of the crust and the upper mantle beneath central Java from local tomography inversion, *J. Geophys. Res.*, *112*, B08310, doi:10.1029/2006JB004712.

Koulakov, I., A. Jakovlev, and B. G. Luehr (2009), Anisotropic structure beneath central Java from local earthquake tomography, *Geochem. Geophys. Geosyst.*, *10*, Q02011, doi:10.1029/2008GC002109.

Le Cloarec, M.-F., and B. Marty (1993), Volatile fluxes from volcanoes, *Terra Nova*, *3*, 17–27.

Lee, H., J. D. Muirhead, T. P. Fischer, C. J. Ebinger, S. A. Kattenhorn, Z. D. Sharp, and G. Kianji (2016), Massive and prolonged deep carbon emissions associated with continental rifting, *Nat. Geosci.*, *9*, 145–149, doi:10.1038/NGEO2622.

Lu, X., A. Watson, A. V. Gorin, and J. Deans (2005), Measurements in a low temperature CO_2-driven geysering well, viewed in relation to natural geysers, *Geothermics*, *34*, 389–410, doi:10.1016/j.geothermics.2005.05.001.

Mazzini, A., G. Etiope, and H. Svensen (2012), A new hydrothermal scenario for the 2006 Lusi eruption, Indonesia. Insights from gas geochemistry, *Earth Planet. Sci. Lett.*, *317*, 305–318, doi:10.1016/j.epsl.2011.11.016.

Mazzini, A., S. Hadi, G. Etipoe, and S. Inguaggiato (2014), Tectonic control of piercement structures in Central Java, Indonesia, AGU Fall Meeting 2014, OS21B-1138.

McLachlan-Karr, J., I. B. Mochtar, and A. Widodo (2009), The energetics of mud volcanoes, in East Java, Indonesia, in *Proceedings from the Fifth Biennial Emergy Conference*, *EMERGY SYNTHESIS 5: Theory and Applications of the Emergy Methodology*, edited by M. T. Brown et al., pp. 101–114, The Center for Environmental Policy Department of Environmental Engineering Sciences, Univ. of Florida, Gainesville, Fla.

Milkov, A. V. (2000), Worldwide distribution of submarine mud volcanoes and associated gas hydrates, *Mar. Geol.*, *167*, 29–42, doi:10.1016/S0025-3227(00)00022-0.

Nurhandoko, B. E. B., R. Kurniadi, A. D. Purnama, M. R. Susilowati Asmarahadi, S. Widowati, M. R. Abda, R. Martha, and E. Fatiah (2016), Integrated subsurface temperature modeling: Case study of East Java Basin, Indonesian petroleum association, Proceedings 40th Annual Convention, IPA16–723-G.

Olivier, J. G., A. F. Bouwman, J. J. M. Berdowski, C. Veldt, J. P. J. Bloos, A. J. H. Visschedijk, P. Y. J. Zandveld, and J. L. Haverlag (1996), Description of EDGAR Version 2.0: A set of global emission inventories of greenhouse gases and ozone-depleting substances for all anthropogenic and most natural sources on a per country basis and on 1 degree x 1 degree grid, IVM, Bilthoven, RIVM Rapport, 771060002. [Availabe at http://www.rivm.nl/bibliotheek/rapporten/771060002.pdf, accessed 02/12/2016.]

Oppenheimer, C., P. Francis, M. Burton, A. J. H. Maciejewski, and L. Boardman (1998), Remote measurement of volcanic gases by Fourier transform infrared spectroscopy, *Appl. Phys. B: Lasers and Optics*, *67*, 505–515.

Poli, S., E. Franzolin, P. Fumagalli, and A. Crottini (2009), The transport of carbon and hydrogen in subducted oceanic crust: An experimental study to 5 GPa, *Earth Planet. Sci. Lett.*, *278*, 350–360.

Putra, S. D. H., Suryantini, and W. Srigutomo (2016), Thermal modeling and heat flow density interpretation of the onshore Northwest Java Basin, Indonesia, *Geotherm. Energy*, *4*, 1–24, doi:10.1186/s40517-016-0052-x.

Queißer, M., D. Granieri, and M. Burton (2016), A new frontier in CO_2 flux measurements using a highly portable DIAL laser system, *Sci. Rep.*, *6*, 33834, doi:10.1038/srep33834.

Roberts, K. S., J. D. Richard, and S. A. Stewart (2011), Structural controls on mud volcano vent distributions: Examples from Azerbaijan and Lusi, East Java, *J. Geol. Soc. London*, *168*, 1013–1030, doi:10.1144/0016-76492010-158.

Roy, G., and L. R. Bissonette (2001), Strong dependence of rain induced lidar depolarization on the illumination angle: Experimental evidence and geometrical-optics interpretation, *Appl. Opt.*, *40*(27), 4770–4789.

Satyana, A. H, and Asnidar (2008), Mud diapirs and mud volcanoes in depression of Java to Madura: Origins, natures and implications to petroleum systems, Proceedings of the Indonesian Petroleum Association, paper presented at 32nd Annual Convention & Exhibition, May 2008, IPA08-G-139.

Satyana, A. H, and E. M. M. Purwaningsih (2003), Oligo-Miocene carbonates of Java: Tectonic setting and effects of volcanism, paper presented at 32nd IAGI and 28th HAGI Annual Convention and Exhibition, Jakarta.

Seewald, J. S., W. E. Seyfried Jr., and W. Shanks (1994), Variations in the chemical and stable isotope composition of carbon and sulfur species during organic-rich sediment alteration: An experimental and theoretical study of hydrothermal activity at Guaymas Basin, Gulf of California, *Geochim. Cosmochim. Acta*, *58*(22), 5065–5082.

Setijadji, L. D. (2010), Segmented volcanic arc and its association with geothermal fields in Java Island, Indonesia, paper presented at World Geothermal Congress, Bali, Indonesia, 25–29 April.

Shinohara, H. (2005), A new technique to estimate volcanic gas composition: Plume measurements with a portable multi-sensor system, *J. Volcanol. Geotherm. Res.*, *143*, 319–333.

Smyth, H., R. Hall, J. Hamilton, and P. Kinny (2005), East Java: Cenozoic basins, volcanoes and ancient basement, Indonesian petroleum association, Proceedings 30th Annual Convention, 251–266, IPA05-G-045.

Smyth, H. R., R. Hall, and G. J. Nichols (2008), Cenozoic volcanic arc history of East Java, Indonesia: The stratigraphic record of eruptions on an active continental margin, in *Formation and Applications of the Sedimentary Record in Arc Collision Zones*, edited by A. E. Draut, P. D. Clift, and D. W. Scholl, *Geol. Soc. Am. Spec Pap.*, 436, pp. 199–222, doi:10.1130/2008.2436(10).

Stoiber, R. E., L. L. Malinconico Jr., and S. N. Williams (1983), *Use of Correlation Spectrometer at Volcanoes, in Forecasting Volcanic Events*, edited by H. Tazieff and J. C. Sabroux, pp. 425–444, Elsiever, New York.

Toutain, J.-P., F. Sortino, J.-C. Baubron, P. Richon, S. S. Surono, and A. Nonell (2009), Structure and CO_2 budget of Merapi volcano during inter-eruptive periods, *Bull. Volcanol.*, *71*, 815–826.

Untung, M., and Y. Sato (1978), *Gravity and Geological Studies in Java*, vol. 6, p. 207–210, Geological Survey of Indonesia and Geological Survey of Japan Special Publication, Indonesia.

Vanderkluysen, L., M. R. Burton, A. B. Clarke, H. E. Hartnett, and J.-F. Smekens (2014), Composition and flux of explosive gas release at LUSI mud volcano (East Java, Indonesia), *Geochem. Geophys. Geosyst.*, *15*, 2932–2946, doi:10.1002/2014GC005275.

Wagner, D., I. Koulakov, W. Rabbel, B.-G. Luehr, A. Wittwer, H. Kopp, M. Bohm, G. Asch, and the MERAMEX Scientists (2007), Joint inversion of active and passive seismic data in Central Java, *Geophys. J. Int.*, *170*, 923–932, doi:10.1111/j.1365-246X.2007.03435.x.

Waltham, D., R. Hall, H. R. Smyth, and C. J. Ebinge (2008), Basin formation by volcanic arc loading, in *Formation and Applications of the Sedimentary Record in Arc Collision Zones*, *Geol. Soc. Am. Spec. Pap.*, *436*, edited by A. E. Draut et al., pp. 11–26, Geol. Soc. Am., Denver, doi: 10.1130/2008.2436(02).

Westbrook, G., and M. J. Smith (1983), Long decollements and mud volcanoes: Evidence from the Barbados ridge complex for the role of high pore-fluid pressure in the development of an accretionary complex, *Geology*, *11*, 279–283.

Wiloso, D. A., E. A. Subroto, and E. Hermanto (2009), Confirmation of the Paleogene source rocks in the Northeast Java Basin, Indonesia, based from petroleum geochemistry, Search and Discovery Article v. #10195.

Whittaker, J. M., R. D. Müller, M. Sdrolias, and C. Heine (2007), Sunda-Java trench kinematics, slab window formation and overriding plate deformation since the Cretaceous, *Earth Planet. Sci. Lett.*, *255*(3), 445–457.